Advanced Composite Materials
Publication details, including instructions for authors and subscription information:
http://www.tandfonline.com/loi/tacm20

Effect of fiber orientation and moisture absorption on the interlaminar fracture toughness of CFRP laminates

Iton Chou [a]

[a] Structure and Strength Department, Research Institute, Ishikawajima-Harima Heavy Industries Co., Ltd., 1-15, Toyosu 3-chome, Koto-ku, Tokyo 135-8732, Japan

Version of record first published: 02 Apr 2012.

To cite this article: Iton Chou (1998): Effect of fiber orientation and moisture absorption on the interlaminar fracture toughness of CFRP laminates, Advanced Composite Materials, 7:4, 377-394

To link to this article: http://dx.doi.org/10.1163/156855198X00264

Adv. Composite Mater., Vol. 7, No. 4, pp. 377–394 (1998)

Effect of fiber orientation and moisture absorption on the interlaminar fracture toughness of CFRP laminates

ITON CHOU *

Structure and Strength Department, Research Institute, Ishikawajima-Harima Heavy Industries Co., Ltd., 1-15, Toyosu 3-chome, Koto-ku, Tokyo 135-8732, Japan

Received 17 June 1998; accepted 21 July 1998

Abstract—This study has clarified the effects of fiber orientation and the moisture content on G_{IC}/G_{IR} (Mode I energy release rate at initiation/propagation) and G_{IIC}/G_{IIR} (Mode II energy release rate at initiation/propagation) in CFRP laminates. The interlaminar fracture toughnesses at the 0/0, 30/−30, 60/−60, 0/90, and the (0/90)/(0/90) plain weave interfaces were measured using the DCB (Double Cantilever Beam) test and the ENF (End Notched Flexure) test. For the 0/0 interface, the interlaminar fracture toughness under dry, 50% relative humidity equilibrium, and wet conditions were also measured. Fiber orientations at delaminated surfaces were found to affect the interlaminar fracture toughness at initiation (G_{IC} and G_{IIC}) slightly, and the interlaminar fracture toughness during propagation (G_{IR} and G_{IIR}) strongly. Also, the degree of moisture absorption affected G_{IC} slightly, anf G_{IR} strongly. In Mode II, G_{IIC} was strongly affected by the degree of moisture absorption. Contrary to this, G_{IIR} was not affected by moisture absorption.

Keywords: Interlaminar; fracture toughness; Mode I; Mode II; fiber orientation; moisture absorption.

1. INTRODUCTION

Advanced composite materials such as Carbon Fiber Reinforced Plastics (CFRP) are often used for aerospace structures because of their high specific strengths and stiffnesses. In these structures, high structural reliability is required. For this reason, it is important in the design stage to determine the failure strength. The design concept on delamination failure, especially for laminated CFRP structures, is needed because delamination failure is a major consideration in such structures.

It is an attractive issue in real laminated structures to measure delamination resistance between differently oriented plies, because designers can choose stacking sequences. There are several works [1–8] which report the interlaminar fracture

*E-mail: iton_chou@ihi.co.jp

toughness measured between differently oriented plies. As well as the effects of fiber orientation, the effects of the moisture absorption on the delamination resistance have been conducted [1, 9–13]. However, a comprehensive study regarding the effects of fiber orientation and the moisture absorption on the delamination resistance were not performed in the works.

The author has investigated delamination resistance in CFRP laminates by conventional interlaminar fracture toughness tests in order to build up an estimation method of delamination growth in laminated composites [14–22]. The works reported the effects of factors, such as the kind of material, fiber orientation at delaminated surfaces and the moisture content, on the interlaminar fracture toughness in CFRP laminates. In this paper, the study is developed to include the effects of fiber orientation and the moisture content on Mode I and Mode II interlaminar fracture toughness obtained from the DCB (Double Cantilever Beam) test and the ENF (End Notched Flexure) test. The effects of fiber orientation and moisture absorption on the interlaminar fracture toughness at initiation and during the propagation stage are summarized in this study.

2. EXPERIMENTAL

2.1. Specimen geometry and fabrication

The materials employed in this study were graphite/epoxy composites supplied by Toray, one of which consisted of continuous unidirectional graphite fibers of Type T800H in a matrix of Type 3631 epoxy, and the other consisted of continuous plain woven graphite fibers of T800H in the same matrix. Composite panels were fabricated in an autoclave using unidirectional prepreg and the plain woven prepreg. They were cured under 294 kPa of pressure at 177°C (350°F) for 2 h. DCB and ENF test specimen geometries are illustrated in Figs 1 and 2. Stacking sequences and the total thickness of film insert were selected as shown in Table 1. In the table, // represents the film insert. Folded double layers of 7.5 μm-thick Kapton film and of 75 μm-thick FEP film (a fluorinated film supplied by Toray) were used for inserting between the two plies in the middle of the specimen to introduce a preset delamination. Type A, B, C, and D test specimens were fabricated using the unidirectional prepreg, and the Type E test specimen was fabricated using the plain woven prepreg. After fabrication, DCB and ENF specimens were cut from each panel. Aluminum end blocks were bonded to the delaminated end of the DCB specimens using an epoxy two-component paste adhesive (Araldite, supplied by Ciba-Geigy). Test specimens such as Type B and Type C were stacked antisymmetrically for the full thickness, but each half of the specimen was stacked symmetrically. Such stacking sequences gave flat fabricated panels, and the test specimens did not torsionally deform in the tests. The fiber volume fraction of specimens fabricated with unidirectional prepreg was approximately 58%, and that of specimens fabricated with plain woven prepreg was approximately 51%.

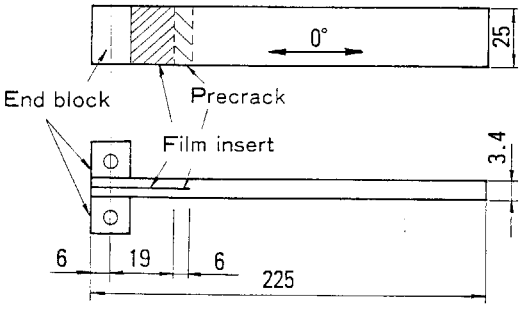

Figure 1. Dimensions of DCB specimen (mm).

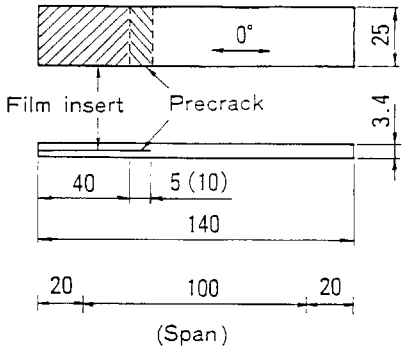

Figure 2. Dimensions of ENF specimen (mm).

Table 1.
Stacking sequences and summary of total thickness of film insert

Test specimen	Stacking sequence	Total thickness of film insert (μm)	
		DCB specimen	ENF specimen
Type A	$[0°_{12}//0°_{12}]$	150	15* 150**
Type B	$[30°/-30°/0°_8/-30°/30°$ $//-30°/30°/0°_8/30°/-30°]$	150	15
Type C	$[60°/-60°/0°_8/-60°/60°$ $//-60°/60°/0°_8/60°/-60°]$	150	15
Type D	$[90°/0°/90°/0°_6/90°/0°/90°$ $//90°/0°/90°/0°_6/90°/0°/90°]$	150	Not fabricated
Type E	$[(0°/90°)_8/(0°/90°)_8]$ (Plain weave)	150	150

* KAPTON (folded): 6 mm precrack (DCB), 5 mm precrack (ENF).
** FEP (folded): 6 mm precrack (DCB), 10 mm precrack (ENF).

The effect of moisture absorption on the interlaminar fracture toughness is shown in Table 1 for Type A specimens. They were, at first, vacuum dried in an oven at 100°C after the pre-cracking was introduced. Type A specimens were then conditioned in a conditioning oven until the moisture content in each specimen reached the 50% equilibrium or saturated condition under the exposure conditions shown in Table 2. Interlaminar fracture toughness tests were performed after completing these processes. In Table 2, Type AD represents test specimens under the dry condition. Type AJ represents test specimens under the equilibrium condition according to Japanese Industrial Standard (JIS K-7100). Type AW represents test specimens under the saturated wet condition. The content of moisture absorption is expressed in terms of weight content. For example, a typical relation between weight content of moisture absorption and the exposure time in Type AW specimens is shown in Fig. 3.

Table 2.
Moisture absorbing conditions of test specimens

Type of specimen	AD	AJ	AW
Condition	Dry	50% equilibrium	Wet
Environmental temperature (°C)	100	23	85
Relative humidity (%)	Vacuum drying	50	98
Exposure time	—	2 weeks (Equilibrium condition)	3 months (Saturated condition)
Moisture absorption (wt%)	0	0.2	1.6

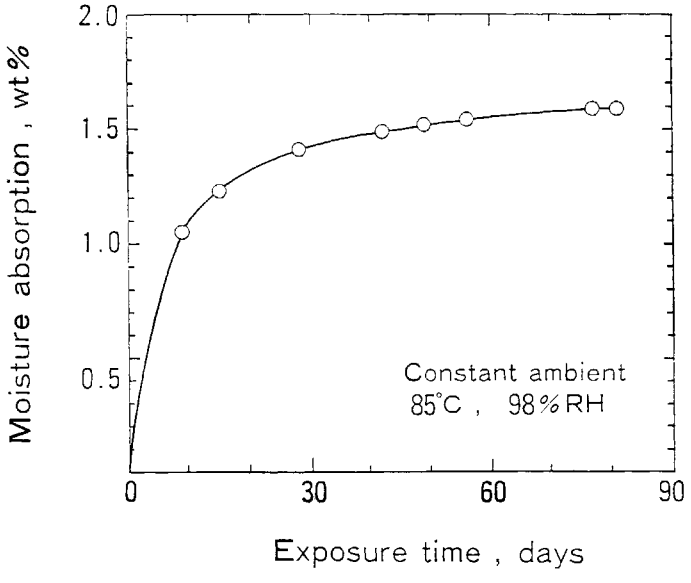

Figure 3. Relationship between moisture content and exposure time for Type AW specimens.

Before performing the DCB and ENF tests, Mode I pre-cracks were introduced using a wedge for all specimens. For the folded FEP film insert, the pre-cracking was introduced after removing the film. For the folded Kapton film insert, the film was not removed. The folded Kapton film was cut in two with a razor blade after introducing the pre-crack. The pre-crack lengths are listed in the footnote of Table 1.

According to the Japanese Industrial Standard, *Testing Methods for Interlaminar Fracture Toughness of Carbon Fiber Reinforced Plastics* (JIS K-7086 in the English version), the pre-crack is introduced to ensure the debonding between the fracture surfaces and the starter film. The starter film is cut in two with a razor blade because of the folded film insert. Another reason why the pre-crack is introduced is to reduce the effect of the resin-rich region at the end of the inserted film. The reasons for introducing the pre-crack were the same as those referred to in JIS K-7086, although the inserted film used in this study was thick.

2.2. DCB test procedure

Tests were performed at a constant crosshead rate of 2 mm/min. The crack length was measured using an optical microscope. One edge of the specimen was coated with a white typewriter correction fluid to monitor the position of the crack tip. Loading and unloading were repeated several times for Type A, B, and C specimens. The unloading was not performed for Type D and E specimens because of a fluctuating crack-propagating rate. In this case, the crack length was measured at intervals of 4-mm increases of the load line displacement. The load line compliance was calculated directly from the load and the displacement corresponding to each crack length. The initial crack length was directly measured after testing from the fracture surface of each specimen broken in two pieces.

2.3. ENF test procedure

Tests were performed with a constant crosshead rate of 3 mm/min. The span was 100 mm. During testing, an approximately 360 μm-thick film with a width of 5 mm was inserted between the upper and lower beams of the ENF specimen at the supporting nose of the delaminated end to decrease the friction between the fracture surfaces. The initial crack length was directly measured after testing from the fracture surface of each specimen broken in two pieces in Mode I propagation.

3. DATA REDUCTION PROCEDURES

3.1. Mode I interlaminar fracture toughness

The data reduction procedure for Mode I interlaminar fracture toughness, i.e. the Mode I energy release rate, was based on JIS K-7086, and is described in detail in [14]. The Mode I energy release rate at crack initiation, G_{IC}, was characterized

using three load values. One was P_{NL}, the loading point which corresponded to the onset of non-linearity in the load *versus* load line displacement curve obtained in the DCB tests. Another one was P_5, the loading point which corresponded to the intersection of the 5% secant line (5% offset line) and the load *versus* load line displacement curve. The remaining one was P_{MAX}, the maximum loading point. For small non-linearity, P_5 was considered equal to P_{MAX}. The Mode I energy release rate in propagation, G_{IR}, was also calculated, and the relation between G_{IR} and the crack extension, that is, G_I from initiation to propagation, was conducted.

3.2. Mode II interlaminar fracture toughness

The data reduction procedure for Mode II interlaminar fracture toughness, i.e. the Mode II energy release rate, was based on JIS K-7086. The Mode II energy release rate at crack initiation, G_{IIC}, was characterized using three load values, as in the previous section. To investigate the sub-critical crack growth region, the Mode II energy release rate in the sub-critical crack propagation, G_{IIR}, was also calculated, and the relation between G_{IIR} and the crack extension, that is G_{II} from initiation to propagation, was conducted. Here, the crack initiation was defined by P_{NL}, and the crack length in the region from P_{NL} up to P_{MAX} was corrected according to JIS K-7086.

4. DCB TEST RESULTS AND DISCUSSION

4.1. Effects of fiber orientation

In the DCB tests, the crack length was monitored using an optical microscope. The Type D specimens were found to delaminate at the $0°/90°$ interface. The delamination in the Type D specimens alternately propagated regularly on the upper and lower $0°/90°$ interfaces through transverse cracks in the $90°$ plies in the middle of the specimen. On the other hand, the delamination in the Type C specimens alternately propagated irregularly between the $60°/-60°$ and the next $60°/-60°$ layers through transverse cracks in $60°$ or $-60°$ plies. These characteristic phenomena corresponded to the serration in load *versus* load line displacement curves. No delamination transfer was observed for Type A, Type B, and Type E specimens.

Table 3 shows the summary of G_{IC} characterized at P_{NL}. In the table, the interlaminar angle for the Type D specimens is expressed [0/90] because of the jagged cracks on the upper and lower $0°/90°$ interfaces as explained previously. It is clear in Table 3 that G_{IC} increases as the fiber orientation of plies at the delaminated surfaces incline away from the delamination direction. G_{IC} for the Type E specimen is the highest, and G_{IC} is almost the same for Type A, Type B, and Type C specimens.

The relationship between G_{IR} and the crack extension for each type of specimen is shown in Figs 4 to 8 summarized in Fig. 9. Rough curves including the same group data are expressed in the figure. In these figures, G_{IR} is plotted with the corresponding measured crack extension.

G_{IR} values for Type A and Type E specimens are almost constant macroscopically during crack propagation. Contrary to this, G_{IR} for Type B, Type C, and Type D specimens increases as the crack propagates. In addition, the rate of increase of G_{IR}

Table 3.
Summary of G_{IC}, Mode I interlaminar fracture toughness at crack initiation. Table indicates mean values. Values in parentheses represent coefficients of variation (C.O.V.). (Effects of fiber orientation)

Test specimen	Interlaminar angles (deg)	G_{IC} (J/m^2)
		Mean (C.O.V.)
Type A	[0/0]	194 (0.068)
Type B	[30/−30]	204 (0.104)
Type C	[60/−60]	218 (0.106)
Type D	[0/90]	285 (0.182)
Type E	[(0/90)/(0/90)] (Plain weave)	517 (0.078)

Number of specimens: Type C, 7; another type, 5 for each.

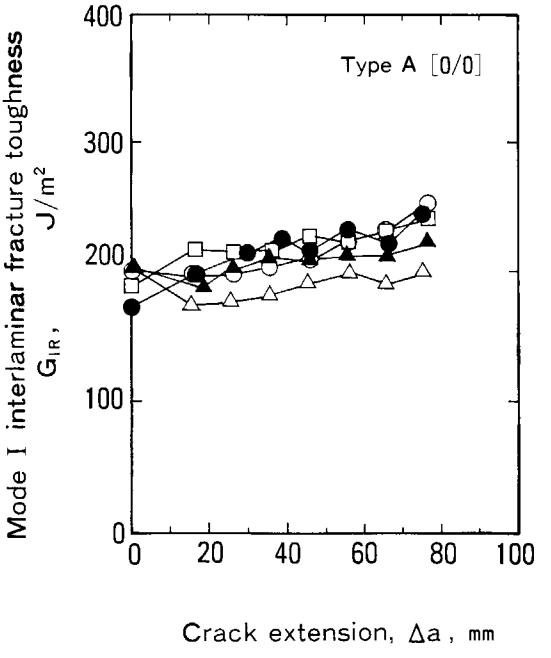

Figure 4. Relationship between Mode I interlaminar fracture toughness, G_{IR}, and crack extension, Δa, for Type A specimens.

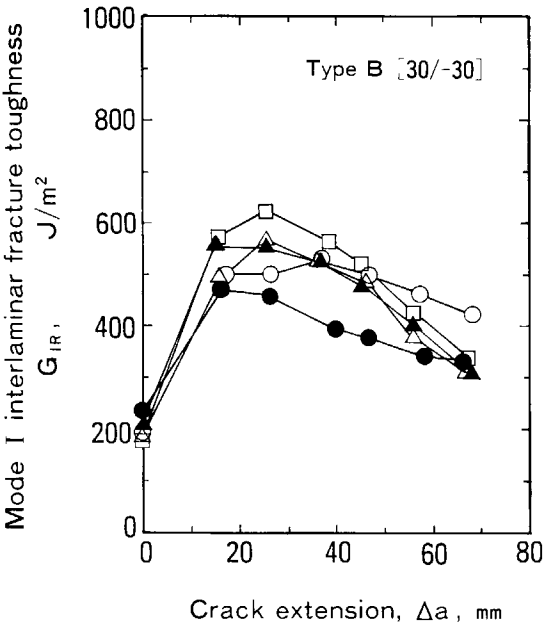

Figure 5. Relationship between Mode I interlaminar fracture toughness, G_{IR}, and crack extension, Δa, for Type B specimens.

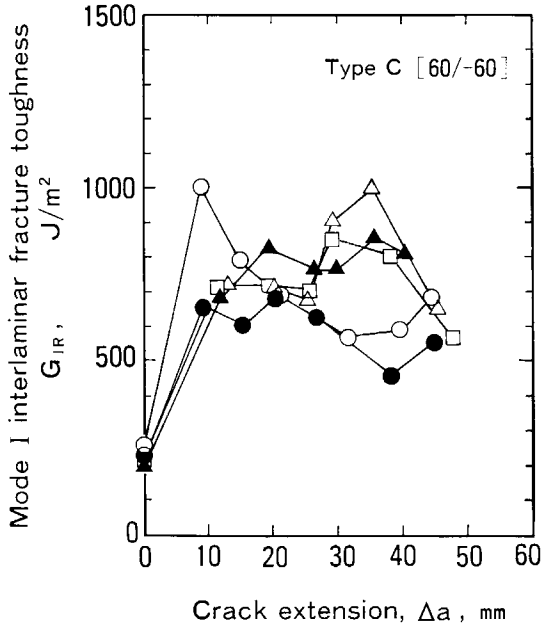

Figure 6. Relationship between Mode I interlaminar fracture toughness, G_{IR}, and crack extension, Δa, for Type C specimens.

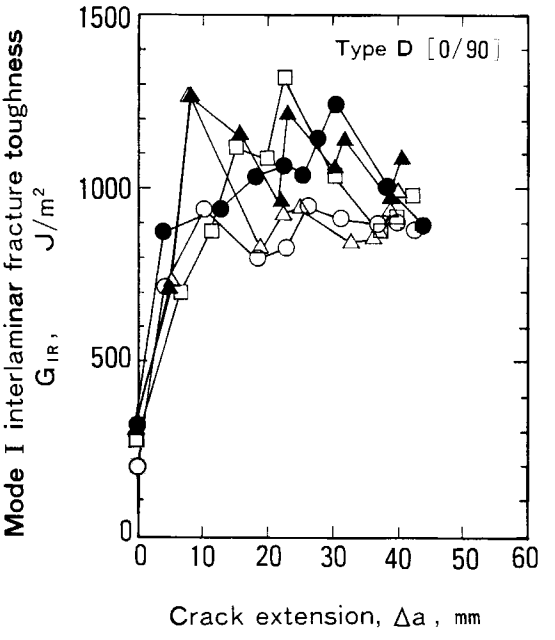

Figure 7. Relationship between Mode I interlaminar fracture toughness, G_{IR}, and crack extension, Δa, for Type D specimens.

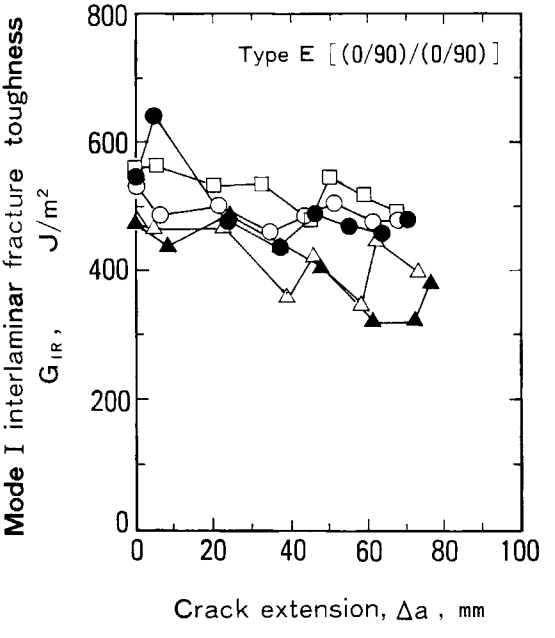

Figure 8. Relationship between Mode I interlaminar fracture toughness, G_{IR}, and crack extension, Δa, for Type E specimens.

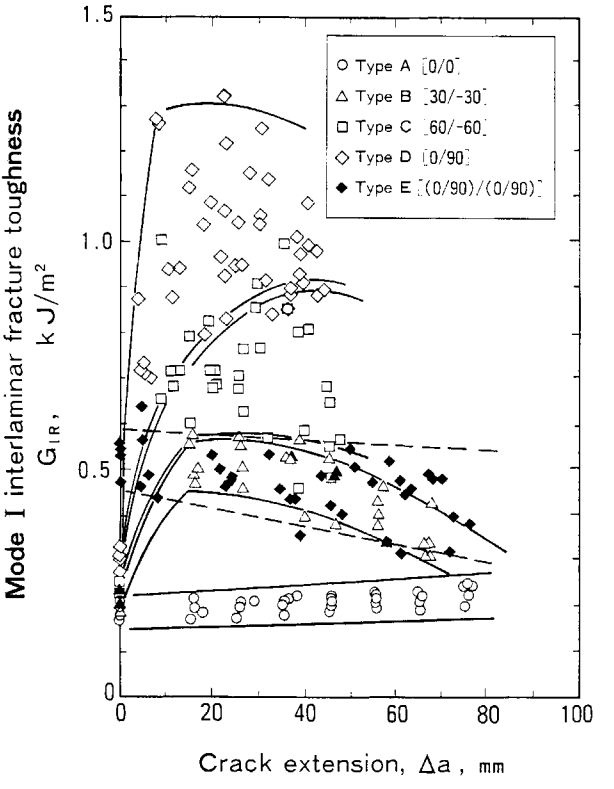

Figure 9. Relationship between Mode I interlaminar fracture toughness, G_{IR}, and crack extension, Δa (effects of fiber orientation).

increases in the order, Type B, Type C, and Type D, respectively. The increase of G_{IR} could be a consequence of the effect of fiber bridging. Another reason for it is the increase of fracture area induced by the transverse cracks observed in Type C and Type D specimens as described previously.

As for the Type B specimens, G_{IR} increases as the crack propagates up to a crack extension of approximately 20 mm, but it gradually decreases thereafter. This is not due to the difference of inserted film layer thickness [21, 22], and is also not due to the kind of materials [22]. One of the reasons that can be proposed for the characteristic phenomenon in the Type B specimens is that the effect of fiber bridging decreases as the crack length becomes long. Another reason is the following; in the case of the delamination at the $30°/-30°$ interface, the fracture mode at the crack front can be considered as locally mixed mode, even though the test specimen deforms macroscopically in Mode I. As the crack length becomes longer, the Mode I component gradually decreases. In this way, G_{IR} gradually decreases as the crack extends. However, further investigation is needed to clarify the mechanism of the phenomenon.

Table 4.
Summary of G_{IC}, Mode I interlaminar fracture toughness at crack initiation and $G_{IR(M)}$, the representative value of Mode I interlaminar fracture toughness during propagation. Table indicates mean values. Values in parentheses represent coefficients of variation (C.O.V.). (Effects of moisture absorption)

Type of specimen	Condition	G_{IC} (J/m^2)			$G_{IR(M)}$ (J/m^2) Propagation
		P_{NL}	P_5	P_{MAX}	
AD	Dry	139 (0.091)	162 (0.059)	182 (0.092)	278 (0.162)
AJ	50% equilibrium (0.2% absorbed)	163 (0.060)	173 (0.048)		190 (0.087)
AW	Wet (1.6 wt% absorbed)	128 (0.079)	161 (0.060)	188 (0.078)	191 (0.87)

4.2. Effects of moisture absorption

Table 4 summarizes the effects of moisture absorption on G_{IC} and $G_{IR(M)}$, the representative value of Mode I interlaminar fracture toughness during propagation. The value of $G_{IR(M)}$ indicates the mean value of G_{IR} in the range of 20 mm to 70 mm crack extension. It is obvious in Table 4 that G_{IC} values under dry and wet conditions are lower than that under the 50% equilibrium condition in the case of characterizing G_{IC} at P_{NL}. It can be estimated that the absorption condition, where G_{IC} is maximum, exists in the case of characterizing G_{IC} at P_{NL}. The wetting between fibers and the resin at crack initiation was poor under dry and wet conditions by the fracture surface observation of test specimens using a Scanning Electron Microscopy (SEM) [16, 22]. The poor wetting between fibers and the resin might cause the deterioration of G_{IC}. Contrary to G_{IC} characterized at P_{NL}, the fracture toughness is not affected by the moisture content in the case of characterizing G_{IC} at P_5 and P_{MAX}. As for $G_{IR(M)}$, the highest value is achieved under the dry conditions.

The relationships between G_{IR} and crack extension for Type AD, Type AJ, and Type AW specimens are shown in Figs 10 to 12, respectively. In the figures, G_{IC} characterized at P_{NL} is plotted using the initial data of interlaminar fracture toughness. It is clear in Fig. 10 that G_{IR} increases as the crack propagates under dry conditions. On the other hand, G_{IR} under the 50% equilibrium condition is almost constant during propagation as shown in Fig. 11. As for test specimens under wet conditions, as shown in Fig. 12, G_{IR} increases at the early stage of propagation, and then it becomes almost constant during propagation.

5. ENF TEST RESULTS AND DISCUSSION

5.1. Effects of fiber orientation

In the ENF tests, the phenomenon of unstable delamination transfer from the $60°/-60°$ interface to the $0°/-60°$ interface in the compressive side of the

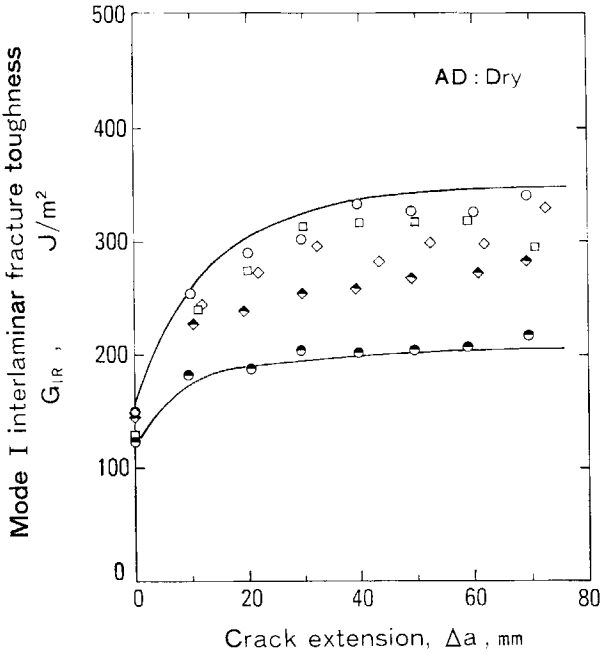

Figure 10. Relationship between Mode I interlaminar fracture toughness, G_{IR}, and crack extension, Δa, for Type AD specimens.

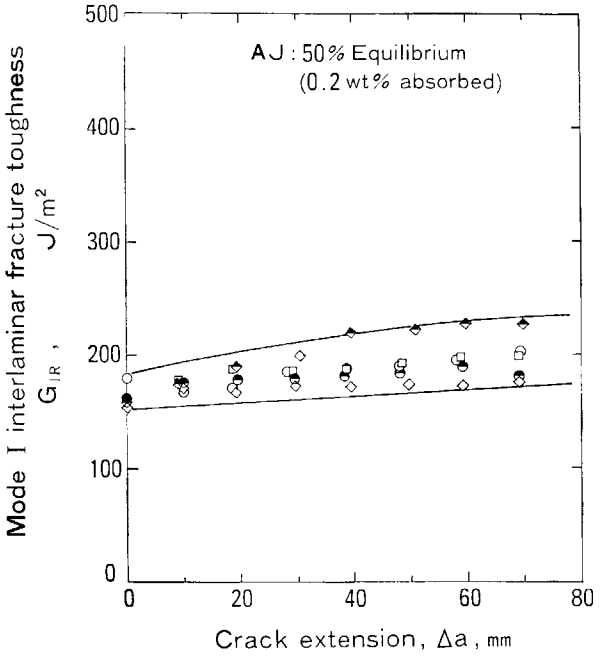

Figure 11. Relationship between Mode I interlaminar fracture toughness, G_{IR}, and crack extension, Δa, for Type AJ specimens.

specimen through transverse cracking in 60° and −60° plies was observed for Type C specimens. The delaminated interface was 60°/−60° at initiation, even though the delamination transfer occurred as explained previously.

Table 5 shows the summary of calculated results for G_{IIC}. It is clear in Table 5 that G_{IIC} increases as the fiber orientation of plies at delaminated surfaces incline

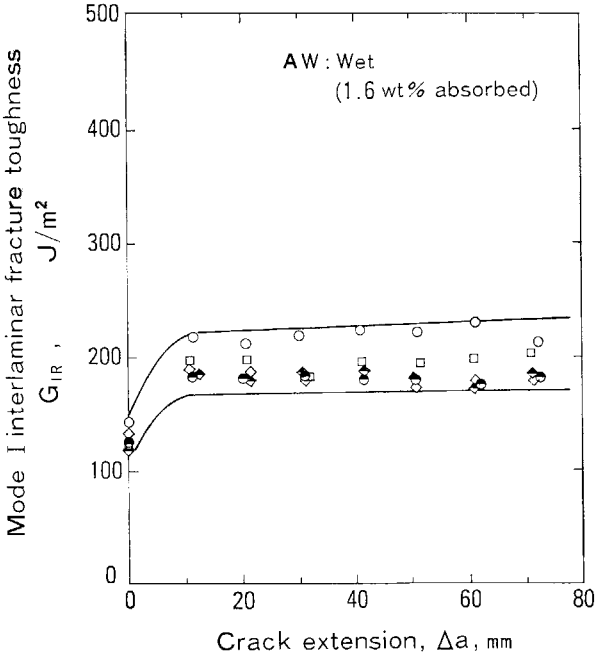

Figure 12. Relationship between Mode I interlaminar fracture toughness, G_{IR}, and crack extension, Δa, for Type AW specimens.

Table 5.
Summary of G_{IIC}, Mode II interlaminar fracture toughness at crack initiation. Table indicates mean values. Values in parentheses represent coefficients of variation (C.O.V.). (Effects of fiber orientation)

Test specimen	Interlaminar angles (deg)	G_{IIC} (J/m²)		
		P_{NL}	P_5	P_{MAX}
Type A	[0/0]	242 (0.059)	507 (0.012)	514 (0.011)
Type B	[30/−30]	184 (0.068)	540 (0.097)	566 (0.137)
Type C	[60/−60]	188 (0.193)	615 (0.186)	624 (0.205)
Type E	[(0/90)/(0/90)] (Plain weave)	313 (0.130)	1110 (0.107)	1644 (0.040)

Number of specimens: Type C, 7; another type, 5 for each.

away from the delamination direction when G_{IIC} is characterized at P_5 and P_{MAX}. G_{IIC} for the Type E specimens was the highest when G_{IIC} is characterized at P_{NL}. The reason for this result may be because the weave at delaminated surfaces is apt to arrest the Mode II deformation, which is related to the increase in delamination resistance. On the other hand, G_{IIC}, for Type A specimen is greater than that for Type B and Type C specimens when G_{IIC} is characterized at P_{NL}. This means that G_{IIC} measured between differently oriented plies is lower than G_{IIC} measured for the $0°/0°$ interface when G_{IIC} is characterized at P_{NL}. An understanding of this fact may be useful in designing a structure with laminated composites, since characterizing G_{IIC} at P_{NL} provides a design with a safety margin.

The relationship between G_{IIR} and the crack extension in the sub-critical crack growth region, which corresponds to the region from P_{NL} up to P_{MAX}, for each type of specimen, is shown in Fig. 13. Comparisons between each type of specimen, rough curves including the same group data, are drawn in the figure. G_{IIR} is plotted with the corresponding calculated crack extension using the equation for the correction of crack length described in JIS K-7086. Here, it was considered that the crack initiation corresponded to P_{NL}. The initiation data of crack length was directly measured, and the crack length in propagation was calculated using the equation described in JIS K-7086.

It is clear in Fig. 13 that G_{IIR} increases as the crack propagates sub-critically. The rate of increase rises in the order, Type A, Type B, Type C, and Type E, respectively. As for Type A and Type E specimens, the tendency of rising G_{IIR} with crack

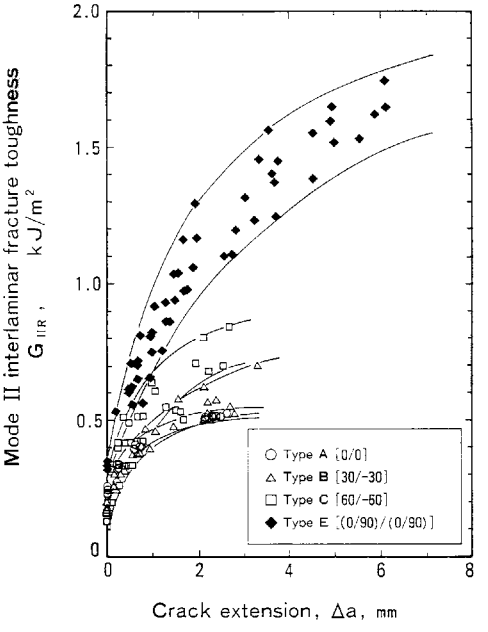

Figure 13. Relationship between Mode II interlaminar fracture toughness, G_{IIR}, and crack extension, Δa (effects of fiber orientation).

extension differs from that of a macroscopically constant G_{IR} with crack extension. One of the reasons for the increase of G_{IIR} may be the effect of the increase of fracture area induced by the transverse cracks observed in Type C specimens as described previously. Another reason for it is because delaminations are apt to be arrested as the fiber orientations of plies at delaminated surfaces incline away from the delamination direction.

5.2. Effects of moisture absorption

Table 6 summarizes the effects of moisture absorption on G_{IIC}. It is obvious in Table 6 that G_{IIC} under the wet condition is lower than those under dry and 50% equilibrium conditions in the case of characterizing G_{IIC} at P_{NL}. The wetting

Table 6.
Summary of G_{IIC}, Mode II interlaminar fracture toughness at crack initiation. Table indicates mean values. Values in parentheses represent coefficients of variation (C.O.V.). (Effects of moisture absorption)

Type of specimen	Condition	G_{IIC} (J/m^2)		
		P_{NL}	P_5	P_{MAX}
AD	Dry	229 (0.083)		627 (0.063)
AJ	50% equilibrium (0.2% absorbed)	239 (0.144)		620 (0.037)
AW	Wet (1.6 wt% absorbed)	194 (0.244)	615 (0.040)	632 (0.053)

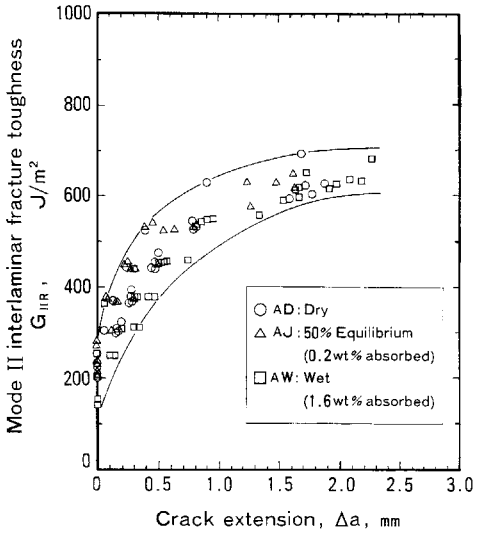

Figure 14. Relationship between Mode II interlaminar fracture toughness, G_{IIR}, and crack extension, Δa (effects of moisture absorption).

between fibers and the resin at crack initiation was poor under the wet condition from the fracture surface observation of test specimens using the SEM [16, 22]. This might cause the deterioration of G_{IIC}. Contrary to G_{IIC} characterized at P_{NL}, the fracture toughness is not affected by the moisture content in the case of characterizing G_{IIC} at P_5 and P_{MAX}.

The relationship between G_{IIR} and crack extension for Type AD, Type AJ, and Type AW specimens are summarized in Fig. 14. In the figure, G_{IIC} characterized at P_{NL} is plotted as the initial data of interlaminar fracture toughness, and the crack length during propagation are calculated using the equation for the correction of crack length as described in JIS K-7086. It is clear in Fig. 14 that G_{IIR} increases as the crack propagates irrespective of the moisture absorbing conditions, and it is not affected by the moisture content. The latter can be explained by the result that no difference, besides the crack initiation, in fracture surfaces of test specimens was observed using the SEM among the three absorbing conditions [16, 22].

6. CONCLUSIONS

Effects of fiber orientation and moisture absorption on Mode I and Mode II interlaminar fracture toughness are described in this paper. Results obtained in this study are summarized in the following.

6.1. Effects of fiber orientation and moisture absorption on G_{IC} and G_{IR}

G_{IC} increases as the fiber orientations of plies at delaminated surfaces inclined away from the delamination direction. G_{IC} for the $(0°/90°)/(0°/90°)$ plain weave interface is the highest, and G_{IC} values for the $0°/0°$, $30°/-30°$ and $60°/-60°$ interfaces are almost the same.

G_{IC} under dry and wet conditions are lower than that under the 50% equilibrium condition in the case of characterizing G_{IC} at P_{NL}. Contrary to G_{IC} characterized at P_{NL}, the fracture toughness is not affected by the moisture content in the case of characterizing G_{IC} at P_5 and P_{MAX}. As for $G_{IR(M)}$, the highest value is attained under the dry condition.

G_{IR} for $0°/0°$ and $(0°/90°)/(0°/90°)$ plain weave interfaces are almost constant macroscopically during crack propagation. Contrary to this, G_{IR} for $30°/-30°$, $60°/-60°$, and $0°/90°$ interfaces increase as the crack propagates. In addition, the rate of increase of G_{IR} increases in the order, $30°/-30°$, $60°/-60°$, and $0°/90°$, respectively. As for the $30°/-30°$ interfaces, G_{IR} increases as the crack propagates up to a crack extension of approximately 20 mm, but it gradually decreases thereafter. This is not due to the difference of inserted film layer thickness [21, 22], and is also not due to the kind of materials [22].

G_{IR} under the dry condition increases as the crack propagates. On the other hand, G_{IR} under the 50% equilibrium condition is almost constant during propagation. G_{IR} under the wet condition increases at the early stage of propagation, and then it becomes almost constant during propagation.

6.2. Effects of fiber orientation and moisture absorption on G_{IIC} and G_{IIR}

G_{IIC} increases as the fiber orientation of plies at delaminated surfaces incline away from the delamination direction when G_{IIC} is characterized at P_5 and P_{MAX}. G_{IIC} for the $(0°/90°)/(0°/90°)$ plain weave interface is the highest when G_{IIC} is characterized at P_{NL}. On the other hand, G_{IIC} measured between differently oriented plies is lower than that measured for the $0°/0°$ interface when G_{IIC} is characterized at P_{NL}.

G_{IIC} values under the wet condition are lower than those under dry and 50% equilibrium conditions in the case of characterizing G_{IIC} at P_{NL}. Contrary to G_{IIC} characterized at P_{NL}, the fracture toughness is not affected by the content of moisture absorption in the case of characterizing G_{IIC} at P_5 and P_{MAX}.

G_{IIR} increases as the crack propagates sub-critically irrespective of fiber orientations at delaminated surfaces. The rate of increase rises in the order, $(0°/0°)$, $30°/-30°$, $60°/-60°$, and $(0°/90°)/(0°/90°)$, respectively.

G_{IIR} increases as the crack propagates irrespective of the moisture absorbing conditions, and it is not affected by the moisture content.

Acknowledgements

The author would like to acknowledge Professors I. Kimpara and K. Kageyama, and Assistant I. Ohsawa at the University of Tokyo for useful discussions and experimental assistance.

REFERENCES

1. A. J. Russell and K. N. Street, Factors affecting the interlaminar fracture energy of Graphite/Epoxy laminates, in: *Proc. ICCM-IV*, pp. 279–286 (1982).
2. D. J. Wilkins, J. R. Eisenmann, R. A. Camin, W. S. Margolis and R. A. Benson, Characterizing delamination growth in Graphyte-Epoxy, in: *ASTM STP 775*, K. L. Reifsnider (Ed.), pp. 168–183. American Society for Testing and Materials, Philadelphia (1982).
3. D. J. Nicholls and J. P. Gallagher, Determination of G_{IC} in angle ply composites using a cantilever beam test method, *J. Reinf. Plast. Compos.* **1**, 2–17 (1983).
4. H. Chai, The characterization of Mode I delamination failure in nonwoven, multidirectional laminates, *Composites* **4**, 277–290 (1984).
5. J. Xiao and S. L. Li, On Mode II delamination fracture toughness of multidirectional interface in composite laminate, in: *Proc. ICCM-VII 2*, pp. 669–674 (1989).
6. J. G. Funk and J. W. Deaton, The interlaminar fracture toughness of woven Graphite/Epoxy composites, NASA TP-2950 (Nov. 1989).
7. A. Laksimi, M. L. Benzeggagh, G. Jing, M. Hecini and J. M. Roelandt, Mode I interlaminar fracture of symmetrical cross-ply composites, *Compos. Sci. Technol.* **41**, 147–164 (1991).
8. P. Robinson and D. Q. Song, A modified DCB specimen for Mode I testing of multidirectional laminates, *J. Compos. Mater.* **11**, 1554–1577 (1992).
9. A. J. Russell and K. N. Street, Moisture and temperature effects on the mixed-mode delamination fracture of unidirectional Graphite/Epoxy, in: *ASTM STP 876*, W. S. Johnson (Ed.), pp. 349–370. American Society for Testing and Materials, Philadelphia (1985).

10. A. J. Russell, K. N. Street and F. Bonsang, Thermal damage effects on delamination toughness of a Graphite/Epoxy composite, *Compos. Sci. Technol.* **32**, 1–14 (1988).
11. A. J. Russell and K. N. Street, Moisture and temperature effects on the Mode I and Mode II interlaminar fracture of Graphite/Epoxy composites, *Key Engng Mater.* **37**, 199–208 (1989).
12. S. Beland, J. P. Komorowski and C. Roy, Hydrothermal influence on the interlaminar fracture energy of Graphite/Bismaleimide modified epoxy composite (IM6/5245C), in: *Proc. ICCM-VI & ECCM-2*, Vol. 3, pp. 305–316 (1987).
13. F. X. de Charentenay, J. M. Harry, Y. J. Prel and M. L. Benzeggagh, Characterizing the effect of delamination defect by Mode I delamination test, in: *ASTM STP 836*, pp. 84–103. American Society for Testing and Materials, Philadelphia (1984).
14. W. T. Chang, I. Kimpara, K. Kageyama and I. Ohsawa, New data reduction schemes for the DCB and ENF tests of fracture-resistant composites, in: *Proc. ECCM-IV*, pp. 503–508 (1990).
15. I. Chou, I. Kimpara, K. Kageyama and I. Ohsawa, Effects of fiber orientation on the mode I interlaminar fracture behavior of CF/EPOXY laminates, *J. Soc. Mater. Sci. Jpn* **467**, 1292–1298 (1992) (in Japanese).
16. I. Chou, I. Kimpara, K. Kageyama and I. Ohsawa, Effects of moisture absorption on mode I and mode II interlaminar fracture toughness of CFRP laminates, *J. Jpn. Soc. Compos. Mater.* **2**, 46–54 (1993) (in Japanese).
17. I. Chou, I. Kimpara, K. Kageyama and I. Ohsawa, Effects of fiber orientation on mode I and mode II interlaminar fracture toughness of CFRP laminates, *J. Jpn. Soc. Compos. Mater.* **3**, 109–119 (1993) (in Japanese).
18. I. Chou, I. Kimpara, K. Kageyama and I. Ohsawa, Interlaminar fracture toughness of CFRP laminates, *Ishikawajima-Harima Engng Rev.* **3**, 158–163 (1993) (in Japanese).
19. I. Chou, I. Kimpara, K. Kageyama and I. Ohsawa, Interlaminar fracture toughness of multidirectional CFRP laminates with toughened epoxy, in: *Proc. Third Jpn Intern. SAMPE Symp.*, pp. 439–444 (1993).
20. I. Chou, I. Kimpara, K. Kageyama and I. Ohsawa, Interlaminar fracture toughness at $+\theta/-\theta$ interfaces in Graphite/Epoxy composites under mixed-mode loading, in: *Proc. ECCM CTS-2*, pp. 617–624 (1994).
21. I. Chou, I. Kimpara, K. Kageyama and I. Ohsawa, Mode I and mode II fracture toughness measured between differently oriented plies in Graphite/Epoxy composites, in: *ASTM STP 1230*, R. H. Martin (Ed.), pp. 132–151. American Society for Testing and Materials, Philadelphia (1995).
22. I. Chou, Research of factors affecting on the interlaminar fracture toughness in carbon fiber reinforced plastics, Doctoral dissertation in the University of Tokyo (Dec. 1996) (in Japanese).